

Ongoing climate change following a complete cessation of carbon dioxide emissions

Nathan P. Gillett^{1*}, Vivek K. Arora¹, Kirsten Zickfeld¹, Shawn J. Marshall² and William J. Merryfield¹

A threat of irreversible damage should prompt action to mitigate climate change, according to the United Nations Framework Convention on Climate Change, which serves as a basis for international climate policy. CO₂-induced climate change is known to be largely irreversible on timescales of many centuries¹, as simulated global mean temperature remains approximately constant for such periods following a complete cessation of carbon dioxide emissions while thermosteric sea level continues to rise¹⁻⁶. Here we use simulations with the Canadian Earth System Model to show that ongoing regional changes in temperature and precipitation are significant, following a complete cessation of carbon dioxide emissions in 2100, despite almost constant global mean temperatures. Moreover, our projections show warming at intermediate depths in the Southern Ocean that is many times larger by the year 3000 than that realized in 2100. We suggest that a warming of the intermediate-depth ocean around Antarctica at the scale simulated for the year 3000 could lead to the collapse of the West Antarctic Ice Sheet, which would be associated with a rise in sea level of several metres^{2,7,8}.

We analyse simulations made with the first-generation Canadian Earth System Model⁹ (CanESM1), which consists of coupled dynamical atmosphere and ocean models with full marine and terrestrial carbon cycle components (see the Methods section). This model reproduces well twentieth-century observations of global mean atmospheric CO₂, as well as its seasonal cycle and interhemispheric gradient⁹. We focus on the climate response to CO₂ alone because it is the longest-lived and most important of the main greenhouse gases, and to simplify the interpretation of our simulations. We first carried out a simulation with prescribed historical and Special Report on Emissions Scenarios (SRES) A2 CO₂ concentration² (HIST/SRES; see the Methods section). Diagnosed cumulative carbon emissions due to land-use change and fossil-fuel sources from this simulation are shown by the black line in Fig. 1a. Two zero-emissions simulations with freely evolving atmospheric CO₂ were initialized from this simulation: one in 2010 when diagnosed cumulative emissions were ~500 PgC (ZE2010), and a second in 2100 when diagnosed cumulative emissions were ~2200 PgC (ZE2100). The ZE2010 simulation may be considered as the most extreme possible mitigation scenario in the absence of any geoengineering.

In the ZE2100 simulation the atmospheric CO₂ concentration declines rapidly following the cessation of emissions for about a century (Fig. 1b), but its rate of decrease is subsequently much slower, and by 3000 over 55% of the atmospheric CO₂ perturbation in 2100 still remains in the atmosphere, approximately consistent with previous results^{1,6}. Global mean temperature

remains almost constant following a cessation of emissions in both simulations¹⁻⁵ (Fig. 2a). The initial rapid decline in atmospheric CO₂ in ZE2100 is driven mainly by ongoing rapid uptake by the terrestrial biosphere^{2,5} (Fig. 1c). As atmospheric CO₂ declines, but temperature stays elevated, the land biosphere begins to give up CO₂ after 2200 (ref. 2). In contrast, the ocean continues to take up CO₂ but at a lower rate after the cessation of emissions^{4,5} (Fig. 1d). Overall the ocean uptake following a cessation of emissions in this model is weaker than in other models whereas the land uptake is stronger^{2,5}, consistent with this model's twentieth-century behaviour⁹. Together these effects lead to a rapid initial decline in atmospheric CO₂ for the first century after emissions cease, but only a slow decline thereafter (Fig. 1b).

Although global mean temperature remains almost constant in ZE2100, there is cooling over the Northern Hemisphere land and Arctic, and pronounced ongoing warming over the Southern Ocean and Antarctica⁵ (Fig. 3c). These temperature changes over the high-latitude oceans are in some cases comparable in magnitude to the temperature changes realized between 1855 and 2105 (Fig. 3a). By the end of the millennium, the largest warming relative to the preindustrial climate, of over 9 °C in places, is simulated around the coasts of Antarctica. As the land has little thermal inertia compared with the ocean, it is reasonable to expect the land to cool in response to the reduction in atmospheric CO₂ while the ocean continues to warm. The Southern Hemisphere response resembles the difference between the equilibrium and transient response to a doubling of CO₂ (ref. 10): the equilibrium response is much larger than the transient response over the high-latitude Southern Ocean, owing to the deep mixing of heat that occurs there. The Arctic Ocean, being relatively small, stably stratified and surrounded by land, seems to be influenced by the cooling of the land surrounding it, and it is here that the largest cooling is simulated in response to an abrupt reduction in atmospheric CO₂ in 2100 (ref. 11). The surface temperature response over the high-latitude oceans is very likely to be amplified by changes in sea ice cover. Arctic ice cover recovers following a cessation of emissions, whereas Antarctic ice cover continues to decrease (Supplementary Fig. S1).

The cooling of the Arctic and warming of the Antarctic after 2100 drive a corresponding pronounced precipitation decrease over the Arctic and a precipitation increase over the Antarctic (Fig. 3d), of comparable magnitude to the moistening in these regions realized before 2100 (Fig. 3b). The warming of the Southern Hemisphere and cooling of the Northern Hemisphere drive a southward shift in the intertropical convergence zone, contributing, for example, to an ongoing drying of parts of North Africa of 20–30% after 2100 (Fig. 3d), in addition to the large drying simulated before 2100 (Fig. 3b). Thus, in some regions the precipitation impacts of anthropogenic carbon dioxide emissions are projected to

¹Canadian Centre for Climate Modelling and Analysis, Environment Canada, University of Victoria, PO 1700, STN CSC, Victoria, British Columbia, V8W 3V6, Canada, ²Department of Geography, University of Calgary, 2500 University Drive N.W. Calgary, Alberta T2N 1N4, Canada.

*e-mail: nathan.gillett@ec.gc.ca.

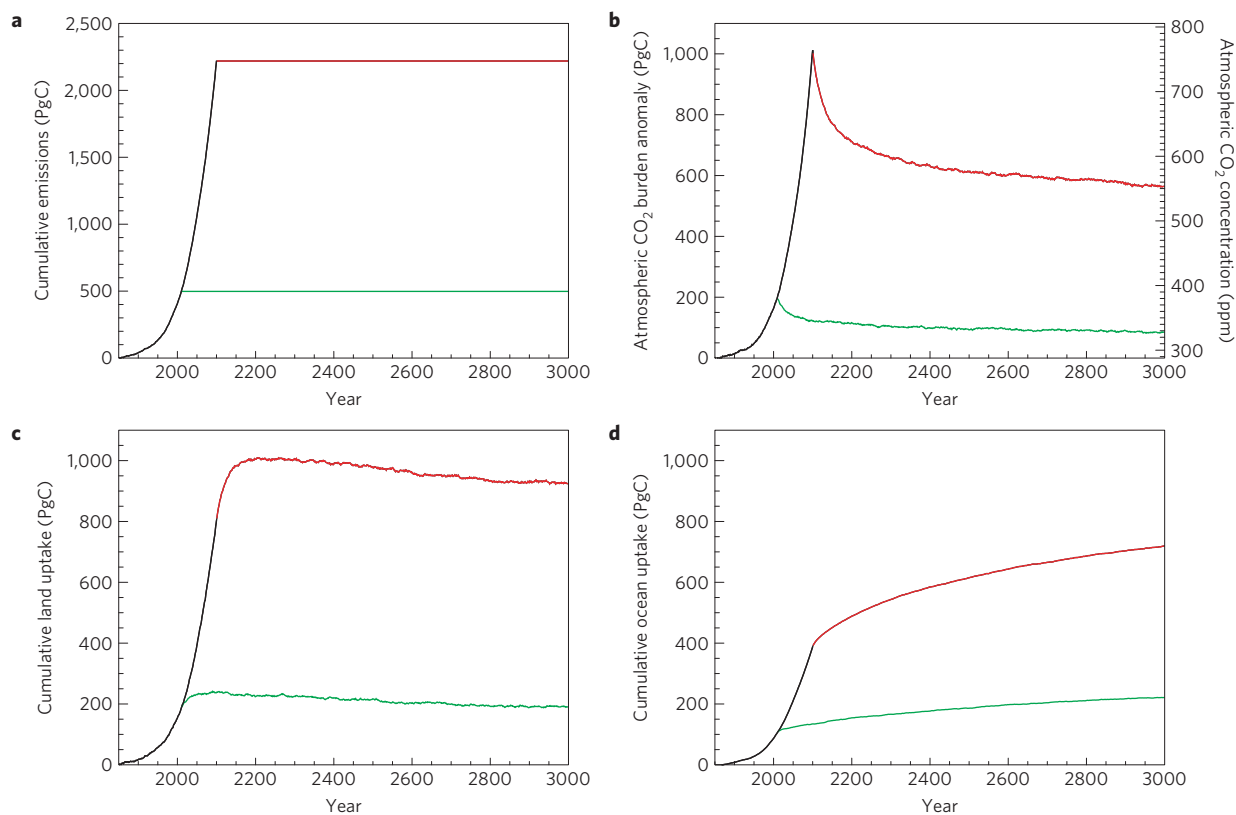


Figure 1 | Carbon dioxide emissions and uptake by the atmosphere, land and ocean. a–d, Diagnosed cumulative CO₂ emissions (a), change in atmospheric CO₂ burden (b), cumulative land carbon uptake (c) and cumulative ocean carbon uptake (d) in the HIST/SRES (black), ZE2010 (green) and ZE2100 (red) simulations, in PgC. Note that b–d have the same vertical scale. The right-hand scale in b shows the atmospheric CO₂ concentration in ppm.

continue to worsen following a cessation of emissions, rather than merely remaining constant¹. Global mean precipitation increases through the ZE2100 simulation, particularly in the first decades after emissions cease (Fig. 2b): such an increase in global mean precipitation is an expected response to decreasing atmospheric CO₂ concentration in the presence of constant global mean surface temperatures^{12,13}, because more efficient radiative cooling to space allows a larger latent heat release in the troposphere.

The ZE2100 simulation exhibits ongoing warming of the ocean between 2100 and 3000, of a maximum of 2.6 °C at 1.4 km depth in the global mean (Fig. 4b), which is larger than the surface-intensified warming realized before 2100 (Fig. 4a). This intensified mid-depth ocean warming is driven primarily by a shift in the deep water formation regions of the North Atlantic to the south and west (Supplementary Fig. S2): the surface temperature averaged over the deep water formation regions of the North Atlantic in March increases by 1.8 °C from 1855 to 2105, and by 4.8 °C from 1855 to 2995, a much larger warming than the increase in global mean sea surface temperature of 2.4 °C over the same period. These changes in the location of the deep water formation regions are driven by a freshening of the Arctic Ocean and East Greenland Current, and the salinification of the subtropical North Atlantic (Supplementary Fig. S3), which are in turn associated with the simulated changes in precipitation (Fig. 3b). Warming of the North Atlantic Deep Water drives a substantial increase in the mid-depth southward heat transport by the end of the simulation (Supplementary Fig. S4), which contributes to the surface warming maximum where these waters upwell in the Southern Ocean (Fig. 3c), and to the overall warming of the Southern Hemisphere and cooling of the Northern Hemisphere after 2100.

The ocean warming results in a thermosteric sea level rise of over 1 m by 3000 in ZE2100, around four times the thermosteric sea

level rise of 25 cm realized by 2100 (ref. 5; Fig. 2c). Even in ZE2010 thermosteric sea level rises by 23 cm by 3000. CanESM1 does not explicitly model the contribution of ice sheets and glaciers to sea level rise. However, the West Antarctic ice sheet is buttressed by ice shelves that are thought to be sensitive to ocean warming at depths of 500–1,000 m, close to the grounding line^{2,7,14}, and because it is grounded below sea level the West Antarctic ice sheet is potentially unstable^{2,7,8,15}. A complete collapse of the Amundsen sector ice sheet would increase global sea levels by ~1.5 m, and a complete collapse of the marine-based portion of the West Antarctic ice sheet would increase global mean sea level by 3–4 m (ref. 16). Observed warming of ~0.2 °C seaward of the Antarctic shelf break is thought to have contributed to rapid thinning of floating ice tongues in the western Amundsen Sea¹⁴, with this thinning propagating inland to give grounding line retreat and ongoing, accelerated ice discharges to the ocean^{17,18}. The last Intergovernmental Panel on Climate Change assessment concludes that a warming of 1 °C under the main West Antarctic ice shelves would eliminate them completely within centuries², removing ice-shelf buttressing effects and facilitating a similar process of grounding line retreat, ice sheet drawdown and increased ice discharge in the Ross and Weddell sea regions.

Figure 4b shows that the simulated warming is intensified in the high-latitude Southern Ocean at 0.5–1.5 km depth in ZE2100. Zonal average ocean temperature at 66° S and 792 m depth warms very little before 2100 but by around 3 °C through the rest of the millennium in ZE2100 (Fig. 2d). This warming of the high-latitude Southern Ocean at intermediate depths is driven by the warming of the North Atlantic Deep Water advected into the Southern Ocean, coupled with a poleward shift in the Deacon cell, and a pronounced weakening of Antarctic Bottom Water overturning cell (Supplementary Fig. S5), allowing these warmer

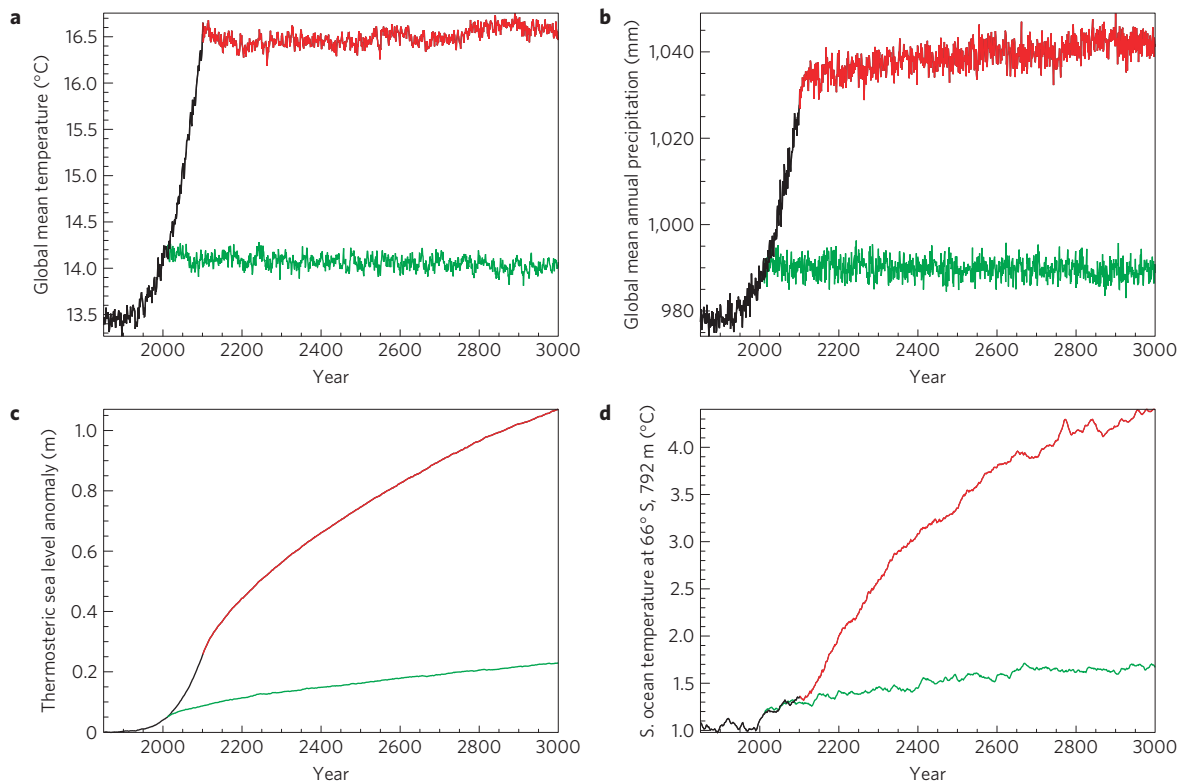


Figure 2 | Time series of the climate response to a cessation of CO₂ emissions. **a–d**, Global mean near-surface air temperature (**a**), global mean precipitation (**b**), global mean thermosteric sea level anomaly (**c**) and zonal mean ocean temperature at 792.5 m, 66° S (**d**) in the HIST/SRES (black), ZE2010 (green) and ZE2100 (red) simulations.

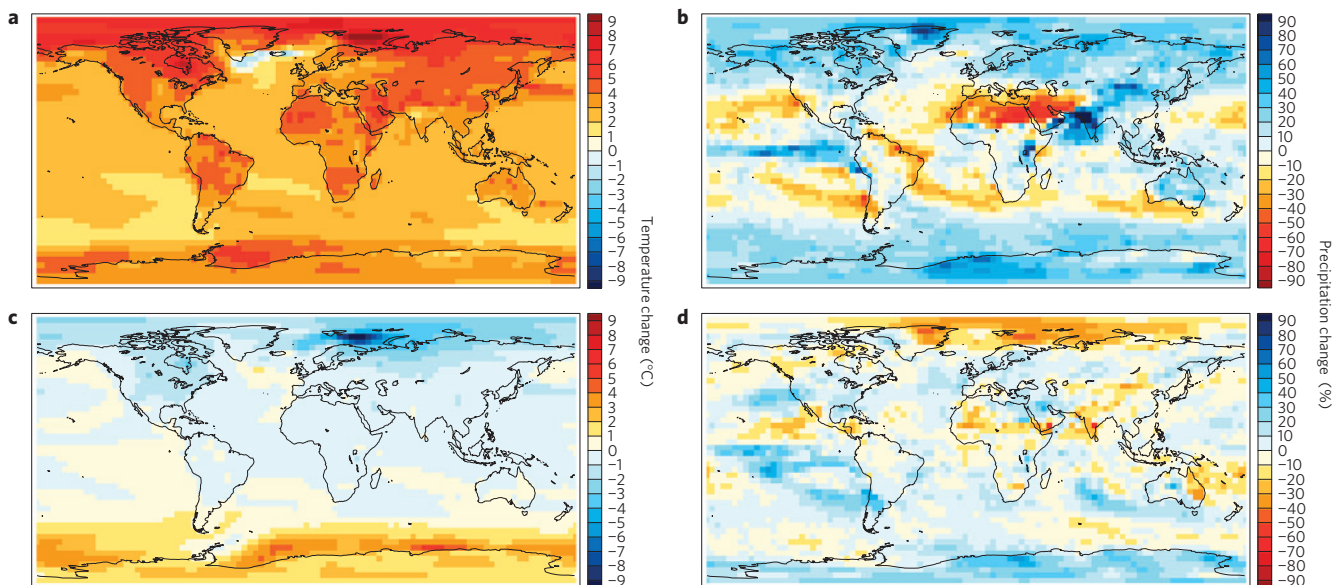


Figure 3 | Simulated patterns of surface temperature and precipitation change before and after a cessation of emissions. **a–d**, Near-surface air temperature change in °C between 1855 and 2105 (**a**), precipitation change between 1855 and 2105 expressed as a percentage of the 1850–1860 mean (**b**), temperature change between 2105 and 2995 (**c**) and precipitation change between 2105 and 2995 (**d**) in HIST/SRES and ZE2100. All changes are calculated as a difference of decadal means centred on the specified years.

waters to approach the Antarctic continent. The Deacon cell shift is in turn driven by a poleward shift in the westerly wind maximum¹⁹, largest in 2100 (Supplementary Fig. S3), and the weakening of Antarctic Bottom Water formation is driven by a much reduced seasonal cycle in Southern Hemisphere sea ice volume (Supplementary Fig. S1). An increase in westerly wind stress

in the high-latitude Southern Ocean (Supplementary Fig. S3) may also contribute to enhanced delivery of warm circumpolar deep water onto the continental shelf²⁰.

Regional ice-sheet/ocean/atmosphere models of coastal Antarctica would be needed to assess the extent to which the warmed circumpolar deep water would reach the ice shelf cavities and

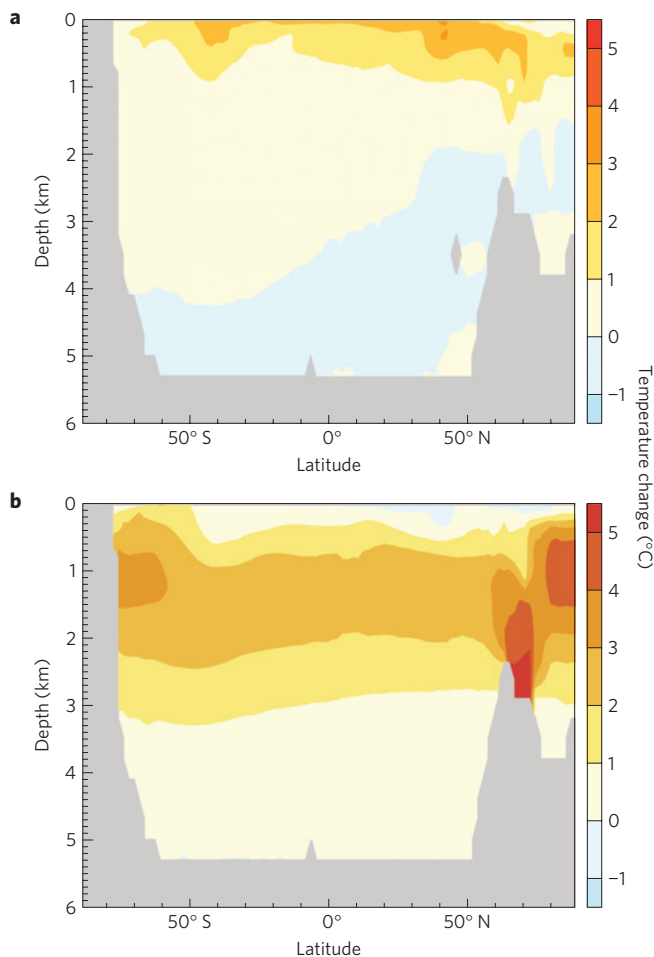


Figure 4 | Ocean temperature change before and after a cessation of emissions. **a, b**, Zonal mean ocean temperature change between 1855 and 2105 (**a**), and between 2105 and 2995 (**b**), in HIST/SRES and ZE2100 (°C).

to quantify the effect that this would have on the ice sheet. Nonetheless, we consider it very likely that the large warming of intermediate-depth water will have an impact on Antarctic ice shelves, and it seems likely that the ice shelves of West Antarctica would be eliminated by the end of the millennium under these conditions. Even in ZE2100 this region of the Southern Ocean warms by $\sim 0.6^\circ\text{C}$ by 3000 (Fig. 2d), suggesting that substantial increased melting of Antarctic ice shelves is already committed based on historical CO_2 emissions. In ZE2100 surface air temperatures over most of Antarctica are simulated to be $4\text{--}6^\circ\text{C}$ warmer than preindustrial by the year 3000, leading to a substantial poleward shift in the -9°C isotherm associated with the limit of ice shelf stability²¹ (Supplementary Fig. S6). This atmospheric warming would be expected to lead to the break-up of several ice shelves in East and West Antarctica, independent of any effects of ocean warming^{22,23}.

Several recent studies have demonstrated that CO_2 -induced global mean temperature change is irreversible on human timescales^{1–6}. We find that not only is this climate change irreversible, but that for some climate variables, such as Antarctic temperature and North African rainfall, CO_2 -induced climate changes are simulated to continue to worsen for many centuries even after a complete cessation of emissions. Although it is also well known that a large committed thermosteric sea level rise is expected even after a cessation of emissions in 2100, our finding of a strong delayed high-latitude Southern Ocean warming at intermediate depths suggests that this effect may be

compounded by ice shelf collapse, grounding line retreat, and ensuing accelerated ice discharge in marine-based sectors of the Antarctic ice sheet, precipitating a sea level rise of several metres. Quantitative results presented here are subject to uncertainties associated with the climate sensitivity, the rate of ocean heat uptake and the rate of carbon uptake in CanESM1, but our findings of Northern Hemisphere cooling, Southern Hemisphere warming, a southward shift of the intertropical convergence zone, and delayed and ongoing ocean warming at intermediate depths following a cessation of emissions are likely to be robust. Geo-engineering by stratospheric aerosol injection has been proposed as a response measure in the event of a rapid melting of the West Antarctic ice sheet²⁴. Our results indicate that if such a melting were driven by ocean warming at intermediate depths, as is thought likely, a geoengineering response would be ineffective for several centuries owing to the long delay associated with subsurface ocean warming.

Methods

CanESM1 is a comprehensive coupled carbon–climate model based on the third-generation atmospheric general circulation model (AGCM3) of the Canadian Centre for Climate Modelling and Analysis⁹, with a horizontal resolution of T47 ($\sim 3.75^\circ$), and 32 layers. The physical ocean component (OGCM3.5) of CanESM1 is based on the National Center for Atmospheric Research (NCAR) community ocean model (NCOM). There is no flux adjustment, and the ocean was spun up for over 1,700 years, such that it exhibited minimal temperature drift. The ocean model is implemented at a horizontal resolution of 1.87° such that there are four ocean grid boxes underlying each atmosphere grid box. There are 29 levels in the vertical and the vertical resolution increases towards the ocean surface, from 300 m in the deep ocean to 50 m in the top 200 m. Atmospheric CO_2 is a fully prognostic three-dimensional tracer in CanESM1 and carbon enters and leaves the atmosphere in the form of anthropogenic emissions and fluxes to or from the underlying land and ocean. The biological and inorganic ocean carbon component of CanESM1 is the Canadian Model of Ocean Carbon (CMOC), which incorporates an inorganic chemistry module (solubility pump) and an ecosystem model (organic and carbonate pumps)²⁵. The ecosystem component of CMOC is based on a nutrient–phytoplankton–zooplankton–detritus (NPZD) model²⁶. Terrestrial ecosystem processes in CanESM1 are modelled using the Canadian Terrestrial Ecosystem Model^{27,28} (CTEM).

An initial simulation was carried out with prescribed fossil-fuel CO_2 emissions²⁹ and land-use change up to 2000, and SRES A2 CO_2 emissions and land-use change from 2001 until 2100. Land-use change emissions were calculated interactively in the model³⁰. To avoid including the effect of land-use albedo changes in our simulations, a second simulation, HIST/SRES, was run from 1850 to 2100 with fixed preindustrial land cover (vegetation type) but using prescribed CO_2 concentrations from our initial simulation. Land cover was also fixed at preindustrial in ZE2100 and ZE2100, though in all simulations the carbon content of the terrestrial biosphere was simulated interactively.

Received 16 July 2010; accepted 10 November 2010;
published online 9 January 2011

References

- Solomon, S., Plattner, G. K., Knutti, R. & Friedlingstein, P. Irreversible climate change due to carbon dioxide emissions. *Proc. Natl Acad. Sci. USA* **106**, 1704–1709 (2009).
- Meehl, G. A. *et al.* in *IPCC Climate Change 2007: The Physical Science Basis* (eds Solomon, S. *et al.*) 747–845 (Cambridge Univ. Press, 2007).
- Matthews, H. D. & Caldeira, K. Stabilizing climate requires near-zero emissions. *Geophys. Res. Lett.* **35**, L04705 (2008).
- Lowe, J. A. *et al.* How difficult is it to recover from dangerous levels of global warming? *Environ. Res. Lett.* **4**, 014012 (2009).
- Frölicher, T. L. & Joos, F. Reversible and irreversible impacts of greenhouse gas emissions in multi-century projections with the NCAR global coupled carbon cycle-climate model. *Clim. Dynam.* **35**, 1439–1459 (2010).
- Eby, M. *et al.* Lifetime of anthropogenic climate change: Millennial time scales of potential CO_2 and surface temperature perturbations. *J. Clim.* **22**, 2501–2511 (2009).
- Walker, D. P. *et al.* Oceanic heat transport onto the Amundsen Sea shelf through a submarine glacial trough. *Geophys. Res. Lett.* **34**, L02602 (2007).
- Thomas, R. H., Sanderson, T. J. O. & Rose, K. E. Effect of climatic warming on the West Antarctic ice sheet. *Nature* **277**, 355–358 (1979).
- Arora, V. K. *et al.* The effect of terrestrial photosynthesis down regulation on the twentieth-century carbon budget simulated with the CCCma earth system model. *J. Clim.* **22**, 6066–6088 (2009).

10. Danabasoglu, G. & Gent, P. R. Equilibrium climate sensitivity: Is it accurate to use a slab ocean model? *J. Clim.* **22**, 2494–2499 (2009).
11. Held, I. M. *et al.* Probing the fast and slow components of global warming by returning abruptly to preindustrial forcing. *J. Clim.* **23**, 2418–2427 (2010).
12. Allen, M. R. & Ingram, W. J. Constraints on future changes in climate and the hydrologic cycle. *Nature* **419**, 224–232 (2002).
13. Yang, F. L., Kumar, A., Schlesinger, M. E. & Wang, W. Q. Intensity of hydrological cycles in warmer climates. *J. Clim.* **16**, 2419–2423 (2003).
14. Rignot, E. & Jacobs, S. S. Rapid bottom melting widespread near Antarctic ice sheet grounding lines. *Science* **296**, 2020–2023 (2002).
15. Katz, R. F. & Worster, M. G. Stability of ice-sheet grounding lines. *Proc. R. Soc. A* **466**, 1597–1620 (2010).
16. Bamber, J. L., Riva, R. E. M., Vermeersen, B. L. A. & LeBrocq, A. M. Reassessment of the potential sea-level rise from a collapse of the West Antarctic ice sheet. *Science* **324**, 901–903 (2009).
17. Payne, A. J., Vieli, A., Shepherd, A. P., Wingham, D. J. & Rignot, E. Recent dramatic thinning of largest West Antarctic ice stream triggered by oceans. *Geophys. Res. Lett.* **31**, L23401 (2004).
18. Velicogna, I. Increasing rates of ice mass loss from the Greenland and Antarctic ice sheets revealed by GRACE. *Geophys. Res. Lett.* **36**, L19503 (2009).
19. Fyfe, J. C., Saenko, O. A., Zickfeld, K., Eby, M. & Weaver, A. J. The role of poleward-intensifying winds on Southern Ocean warming. *J. Clim.* **20**, 5391–5400 (2007).
20. Thoma, M., Jenkins, A., Holland, D. & Jacobs, S. Modelling circumpolar deep water intrusions on the Amundsen Sea continental shelf, Antarctica. *Geophys. Res. Lett.* **35**, L18602 (2008).
21. Morris, E. M. & Vaughan, D. G. in *Antarctic Peninsula Climate Variability: Historical and Paleoenvironmental Perspectives* (eds Domack, E. W. *et al.*) 61–68 (Antarctic Research Series, Vol. 79, American Geophysical Union, 2003).
22. Vaughan, D. G. & Doake, C. S. M. Recent atmospheric warming and retreat of ice shelves on the Antarctic Peninsula. *Nature* **379**, 328–331 (1996).
23. Scambos, T. A., Hulbe, C., Fahnestock, M. & Bohlander, J. The link between climate warming and break-up of ice shelves in the Antarctic Peninsula. *J. Glaciol.* **46**, 516–530 (2000).
24. Blackstock, J. J. *et al.* Climate engineering responses to climate emergencies. *Novim* Preprint at <http://arxiv.org/pdf/0907.5140> (2009).
25. Zahariev, K., Christian, J. R. & Denman, K. L. Preindustrial, historical, and fertilization simulations using a global ocean carbon model with new parameterizations of iron limitation, calcification, and N₂ fixation. *Prog. Oceanogr.* **77**, 56–82 (2008).
26. Denman, K. L. & Peña, M. A. A coupled 1-D biological/physical model of the northeast subarctic Pacific Ocean with iron limitation. *Deep-Sea Res II* **46**, 2877–2908 (1999).
27. Arora, V. K. Simulating energy and carbon fluxes over winter wheat using coupled land surface and terrestrial ecosystem models. *Agric. Forest Meteorol.* **118**, 21–47 (2003).
28. Arora, V. K. & Boer, G. J. A parameterization of leaf phenology for the terrestrial ecosystem component of climate models. *Glob. Change Biol.* **11**, 39–59 (2005).
29. Marland, G., Boden, T. A. & Andres, R. J. in *Trends: A Compendium of Data on Global Change*. (Carbon Dioxide Information Analysis Center, Oak Ridge National Laboratory, 2008).
30. Arora, V. K. & Boer, G. J. Uncertainties in the 20th century carbon budget associated with land use change. *Glob. Change Biol.* **16**, 3327–3348 (2010).

Acknowledgements

We thank S. Solomon, C. Curry and G. Boer for their comments and advice on the manuscript. We thank W. Lee and D. Yang for assistance with processing model output.

Author contributions

N.P.G. designed the experiment, analysed model output, and wrote most of the paper. V.K.A. carried out the CanESM1 simulations, and wrote part of the Methods section. K.Z. contributed to the experimental design and analysis. S.J.M. contributed text and expertise on ice sheet implications. W.J.M. analysed ocean model output and contributed expertise on ocean changes.

Additional information

The authors declare no competing financial interests. Supplementary information accompanies this paper on www.nature.com/naturegeoscience. Reprints and permissions information is available online at <http://npg.nature.com/reprintsandpermissions>. Correspondence and requests for materials should be addressed to N.P.G.